B. Cirera, B. de la Torre, D. Moreno et al. On-surface synthesis of gold porphyrin derivatives via a cascade of chemical interactions: planarization, self-metalation, and intermolecular coupling. Chem. Mater. 31(9), 3248-3256 (2019). DOI: 10.1021/acs.chemmater.9b00125

https://pubs.acs.org/doi/10.1021/acs.chemmater.9b00125

On-surface Synthesis of Gold Porphyrins Derivatives via Cascade of Chemical Interactions: Planarization, Self-metalation and Intermolecular Coupling

Borja Cirera[1,||], Bruno de la Torre[2,3,||], Daniel Moreno[1], Martin Ondráček[2], Radek Zbořil[3], Rodolfo Miranda[1,4], Pavel Jelínek[,2,3], and David Écija*[,1]*

[1]IMDEA Nanoscience, Cantoblanco, Madrid, Spain.

[2] Institute of Physics, The Czech Academy of Sciences, Prague, Czech Republic

[3] Regional Centre of Advanced Technologies and Materials, Palacký University, Olomouc, Czech Republic

[4]Departamento de Física de la Materia Condensada, Universidad Autónoma de Madrid, Cantoblanco, Madrid, Spain.

* jelinekp@fzu.cz; david.ecija@imdea.org

ABSTRACT

On-surface chemistry in ultra-high vacuum offers complementary routes to synthesize molecular complexes which are not accessible through standard solution chemistry. Presence of surface not only impose spatial 2D confinement, but frequently acts as source of adatoms actively participating in the chemical reactions. Here we demonstrate the formation of gold porphyrins derivatives via thermally induced chemical transformations of a fluorinated free-base porphyrin, 2H-4FTPP, on an Au(111) surface, which are rarely accessible via standard protocols of solution chemistry. We also provide accurate description of the mechanisms of on-surface reactions and self-assembly processes, including structural and electronic characterization of intermediates and products using high-resolution scanning probe microscopy with CO-tip supported by computational study. An initial annealing step at 500 K induces planarization of the adsorbed free base via dehydrogenation and ring-closing reactions that preserve the integrity of the C-F bonds. A second annealing step at 575 K enables metalation, producing unprecedented surface-supported gold-coordinated planarized porphyrins (Au-4FPP). A final annealing step at 625 K induces C-F and C-H activation, leading to intermolecular C-C coupling between phenyl termini to form planarized porphyrin oligomers. These results open new avenues for engineering step-wise thermally sensitive on-surface chemical reactions and metal-organic compounds not accessible in solution chemistry.

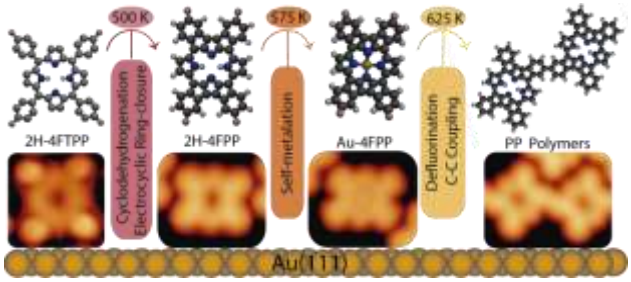

INTRODUCTION

Rational strategies for designing molecular systems on surfaces and controlling their chemical transformations and nanostructures are needed to further our understanding of on-surface chemistry and to support the development of molecule-based devices.[1]

Porphyrins are extraordinary compounds that play central roles in biological processes including metabolism, respiration, and photosynthesis. They have also attracted great interest due to their potential applications in molecular sensing, catalysis, spintronics and nanomagnetism.[2-3]

Because of their importance, many studies conducted in the last two decades have examined the self-assembly of porphyrin derivatives on various surfaces.[4-19] Despite there is some research about the reactions they undergo on surfaces when activated by external stimuli,[19-29] detailed structural data on the products of these reactions[30] and their conformations are needed to understand the chemical reactions, but are very scarce.[31]

In parallel to the studies on porphyrin self-assembly on surfaces, there have been many efforts to modify the physicochemical properties of surface-confined porphyrin derivatives *in situ* by macrocycle metalation.[32-33] However, self-metalation of porphyrins on gold surfaces has been elusive, presumably because of the inertness of the substrate. Furthermore, no chemical transformations of gold porphyrin derivatives on surfaces have been reported. The lack of studies on these processes is surprising given the growing importance of gold porphyrins, which are strong electron acceptors that have applications as photoinduced photosensitizers[34-35] and catalysts,[36] and are becoming increasingly relevant in chemotherapy and anti-HIV treatments.[37-40]

Here we report a comprehensive study on the chemical transformations of the fluorinated free base 5,10,15,20-Tetrakis(4-fluorophenyl)porphyrin, to be termed 2H-4FTPP, on Au(111) induced by three sequential annealing steps (see Sketch 1). The free base porphyrin and its chemical transformations were characterized by low-temperature scanning tunneling microscopy (STM) and high-resolution non-contact atomic force microscopy (nc-AFM) with a CO tip,[41-42] complemented with theoretical calculations. 2H-4FTPP bears fluorine substituents on its peripheral phenyl rings, giving it sufficient thermal stability to undergo sequential intramolecular transformations (planarization and metalation) before participating in intermolecular coupling via activation of its C-F and C-H bonds.[43] This enables stepwise thermal control of its reactivity on Au(111) surfaces.

We show that despite its fluorination, the electronic properties and initial self-assembly behavior of 2H-4FTPP are very similar to those of its non-fluorinated counterpart 2H-TPP when adsorbed on Au(111) at room temperature. Upon annealing, 2H-4FTPP on Au(111) initially undergoes a planarization process involving dehydrogenation and electrocyclic ring closure. The peripheral fluorine substituents are preserved during this process that forms four distinct products, one of which is much more abundant than the others. The resulting fluorinated planarized species establish intermolecular C-H···F-C interactions that cause their self-assembly into novel porphyrin-based one-dimensional supramolecular wires. The second step of the annealing process involves an unprecedented surface-assisted self-metalation of the planarized porphyrins with gold. The third and final step of the annealing process is an on-surface coupling between monomers, which is shown to occur via intermolecular C-C coupling between phenyl moieties resulting from the thermal activation of the C-H and C-F bonds of the pendant phenyl rings. This process forms oligomers incorporating both gold-metalated and metal-free porphyrins.

These results reveal new ways to control intra- and intermolecular chemical reactions on surfaces and to characterize reaction products, expanding our ability to create tailored porphyrin derivatives and nanoarchitectures on technologically relevant supports.

RESULTS AND DISCUSSION

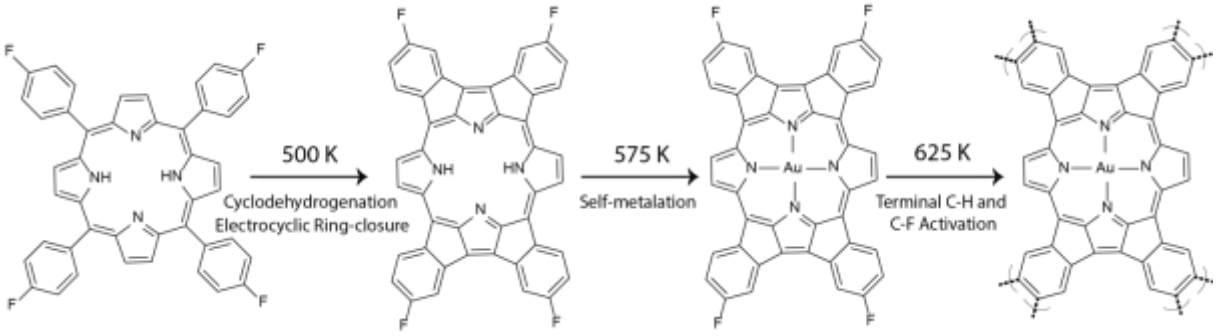

Chemical sketch 1. Thermal reaction pathways of 2H-4FTPP on Au(111) affording: *(i)* Planarization of the molecular backbone via cyclodehydrogenation and electrocyclic ring closure, *(ii)* self-metalation with an Au atom from the Au(111) surface, and *(iii)* terminal C-H and C-F activation.

Chemical sketch 1 shows the free-base porphyrin 2H-4FTPP, which was used as the molecular precursor in this study. Importantly, this compound is functionalized with fluorine substituents on its pendant phenyl rings. In wet chemistry, the high electronegativity and small atomic radius of fluorine are exploited to modulate the electronic properties of macrocyclic ligands without inducing large structural deformations. In this work, a fluorinated precursor was used to compare the activation of C-H and C-F bonds, as discussed below.

The deposition of a submonolayer coverage (0.5 ML) of 2H-4FTPP species on Au(111) at room temperature gives rise to spatially extended closed-packed islands (cf. Fig.1a), highlighting the high mobility of the species (cf. Figure 1a). The high resolution image shown in Figure 1b indicates that the self-assembled structure can be described by a rectangular unit cell ($|\vec{a}|$ = 14.4 ±

0.5 Å, $|\vec{b}|$ = 14.0 ± 0.5 Å, enclosing angle of the unit cell vectors β = 92 ± 1º), which is very similar to the structure formed by the analogous non-fluorinated compound 2H-TPP.[18, 44] Each molecule exhibits the characteristic two-fold symmetry resulting from the deformation of the porphyrin macrocycle upon surface confinement.[2] The inner depression is assigned to the free-base macrocycle, while the four terminal protrusions are attributed to the fluorinated aryl moieties. The saddle-shaped deformation of the adsorbed porphyrins is clearly visible in the nc-AFM and constant height images (cf. Figure 1c,d).

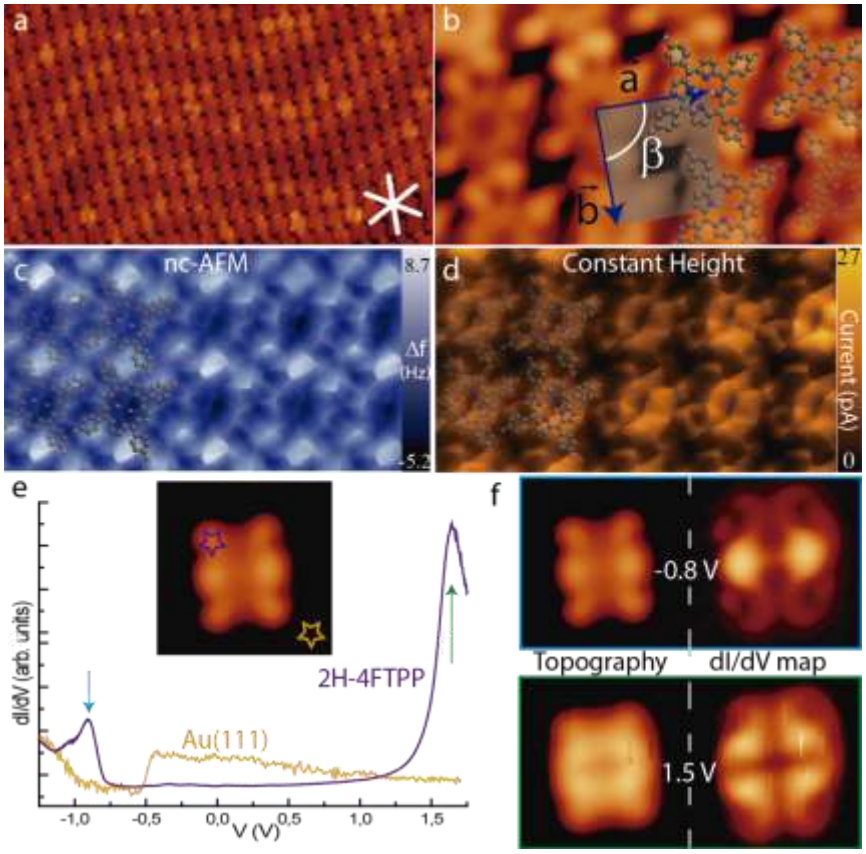

Figure 1. Self-assembly and electronic structure of 2H-4FTPP species on Au(111). a) Long-range STM image of the close-packed assembly. b) High resolution STM topography of the close-packed rectangular nanoarchitecture, highlighting the unit cell (blue vectors) and intramolecular features. c) nc-aFM image showing the non-planarity of the intact 2H-4FTPP species. d) Current map at constant height (feedback-loop open) acquired simultaneously with image c). e) STS spectra recorded on the pristine Au(111) substrate (yellow) and over one corner of an intact adsorbed 2H-4FTPP molecule (purple). The spectrum of the adsorbed molecule features resonances at ca. -0.9 and 1.6 eV. Setting parameters for STS: I_t= 250 pA, V_b= -0.9 V, $V_{modulation}$ = 10 mV, frequency= 773 Hz, integration time per point = 36 ms, sampling

energy= 3.0 meV. f) Topography (left) and associated dI/dV maps at constant current (right) recorded at the approximate energies of the two resonances. Setting parameters for dI/dV maps: I_t = 180 pA, $V_{modulation}$= 10 mV, integration time per point = 10 ms. Image size: a) 30 × 17 nm^2, b) 5.0 × 2.8 nm^2, c-d) 7.0 × 3.9 nm^2, f) 2.0 × 4.2 nm^2. Tunneling parameters: a) V_b = 0.7 V, I_t = 50 pA ; b) V_b = 0.7 V, I_t = 500 pA; d) V_b = 10 mV, R_t~1 GΩ.

The electronic structure of the adsorbates was investigated by scanning tunneling spectroscopy, which revealed two clear resonances at -0.9 and 1.6 eV (cf. Figure 1e). By comparison to the STS spectra of other surface-confined tetrapyrrole derivatives, these resonances were assigned unambiguously to the HOMO and LUMO of the species, revealing that the HOMO-LUMO gap of 2H-4FTPP on Au(111) is around 2.5 eV. This value is consistent with that determined for 2H-TPP on Au(111),[18] demonstrating that the fluorine substituents have little effect on the overall electronic structure of the molecule. To visualize the spatial distribution of the frontier orbitals, constant current dI/dV maps were acquired at the targeted bias voltages for the isolated species (see Figure 1f, right-hand panels). The HOMO appears to have a bowtie shape while the LUMO has a four-lobed flower shape, both of which are again consistent with observations of other free-base porphyrins on Au(111).[45]

Annealing a submonolayer coverage of 2H-4FTPP (0.5 ML) on Au(111) at 500 K resulted in the formation of one-dimensional supramolecular chains (cf. Figure 2a,b) that were stabilized by intermolecular C-H···F-C interactions. Monomers could be displaced from these chains, creating tailored architectures as shown in Figure SI1. Atomistic models indicated that the mean distance between a fluorine atom and the nearest terminal hydrogen was 2.1 ± 0.4 Å.[46] The STM images suggested that the annealing process planarized the molecular precursors by inducing dehydrogenation and electrocyclic ring closure of their aryl termini and macrocyclic pyrroles, giving rise to four planarized porphyrin species (PPs) designated A, B, C and D; A was the major

product. The observation of a predominant species is consistent with DFT calculations, which indicated that species A has the lowest total energy of the possible PPs (cf. Figure SI2).

The chemical structures and appearances of the four PPs products were determined by analogy to similar PPs synthesized on silver surfaces[26, 47] (cf. Figure 2c). The occurrence of planarization was unambiguously demonstrated by high-resolution STM and nc-AFM with a CO-tip, as shown in Figures SI3, SI4, and 3. Annealing at temperatures slightly below 500 K allowed us to observe various partially planarized intermediates in which one, two, or three phenyl units remained unconverted and were observed to be out-of-plane by STM and nc-AFM (cf. Figures SI3 and SI4).

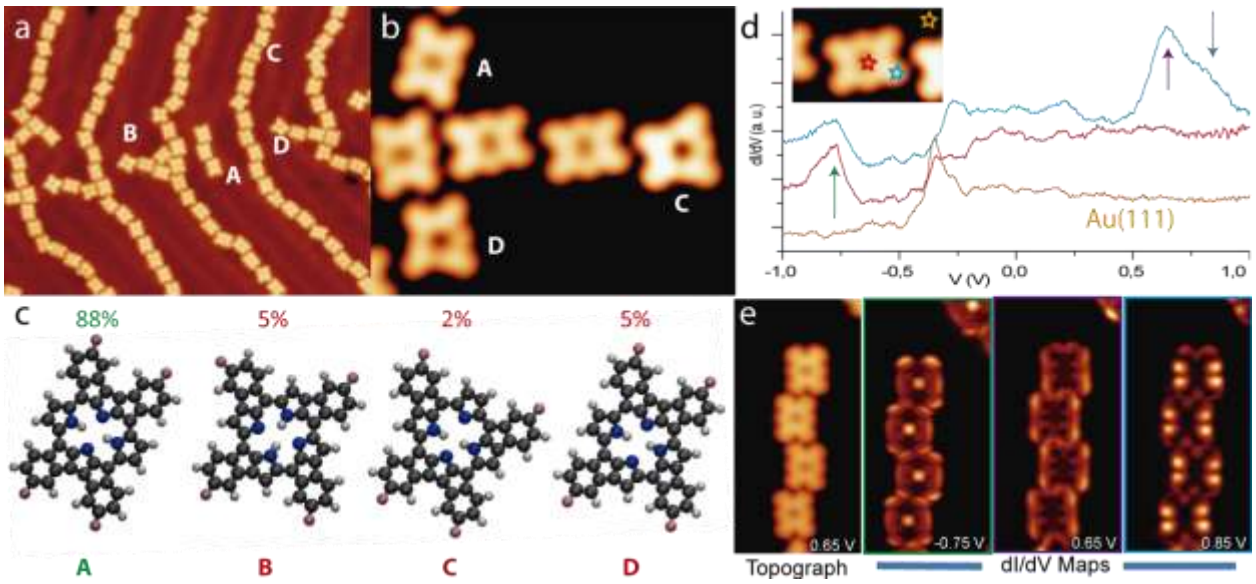

Figure 2. Planarization and self-assembly of porphyrin derivatives upon annealing of 2H-4FTPP on Au(111). a) Long-range STM image showing the four distinct products, labelled A, B, C and D, forming a 1D supramolecular chain. b) Zoomed-in image of a supramolecular chain. c) Ball-and-stick models of the planarized species showing their relative abundances (± 1% error), with A representing the major planarized species. d) STS spectra of the major species A; the red and blue stars in the inset image indicate the points at which the spectra plotted in red and blue were acquired. Setting parameters for STS: I_t = 300 pA, V_b = -1 V, $V_{modulation}$ = 10 mV, frequency = 773 Hz, integration time = 36 ms per point, sampling energy= 2.0 meV. e) Zoomed-in topography of four monomers with the associated constant current dI/dV maps recorded at approximately the energy of the resonances observed in d). Setting parameters for dI/dV maps: I_t = 500 pA, integration time= 12 ms, $V_{modulation}$ = 10 mV. Image size: a) 35 × 27 nm^2, b) 6.0 × 4.7 nm^2, e) 4.25 × 8.5 nm^2. Tunneling parameters: a) V_b = 0.1 V, I_t = 50 pA; b) V_b = -0.7 V, I_t = 120 pA.

Planarization profoundly affected the porphyrin derivatives' electronic structures, changing both the energies and the shapes of their frontier orbitals. Figure 2d shows the dI/dV spectra of the planarized A-type species, revealing a HOMO peak at -0.75 eV and a LUMO peak at ca. 0.65 eV. These values correspond to an energy gap of approximately 1.4 eV, which is around 1 eV lower than that for 2H-4FTPP. Notably, there is a shoulder peak at 0.85 eV. Constant current dI/dV maps (cf. Figure 2e) were acquired to visualize the spatial distribution of the LDOS at the approximate energies of the resonances. The HOMO peak at negative bias exhibited strongly localized electronic states at the peripheral fluorophenyl units and at the center of the cavity, whereas the LUMO was mostly located along the laterals of the long molecular axis. The resonance at 0.85 eV was tentatively assigned to the LUMO+1, which had a distinctive appearance with the charge density being located close to the protonated pyrrole moieties.

Figure 3 shows experimental nc-AFM images of a supramolecular chain consisting of four planarized A-type molecules. These images and the DFT calculations of compound A confirm the complete planarization of the annealed porphyrin derivatives, which together with DFT simulations confirm the full geometrical planarization of the species. The region of C-F bonds at the periphery of molecules features characteristic long rods for certain tip-sample distances (cf. Figure 3a,b). In addition, DFT calculations of the total energy of compound A indicate that the two tautomeric configurations of its inner protons are not energetically equivalent (cf. Figure SI2). Consequently, its tautomeric switching is quenched and these protons are fixed, explaining the asymmetric contrast of the macrocycles seen in high-resolution nc-AFM images (cf. Figure 3c).

To better understand these experimental observations, we performed simulations based on selected AFM images using probe particle code. The excellent agreement between the experimental images (see Figure 3a-c) and nc-AFM simulations of a 2H-4FPP species (see Figure 3d,e) demonstrated the integrity of the C-F bonds (which are visualized as the previously mentioned long rods) and the survival and fixed position of the pyrrolic protons, as shown in Figure 3d. Both constant height high resolution nc-AFM images (Figure 3c) and constant height/current topographs (cf. Figure 4) indicate the presence of a void in the center of the macrocycle, so the faint protrusion observed in the dI/dV maps at -0.75 eV in Figure 2e is assigned to an electronic feature of the planarized species rather than being indicative of metalation.

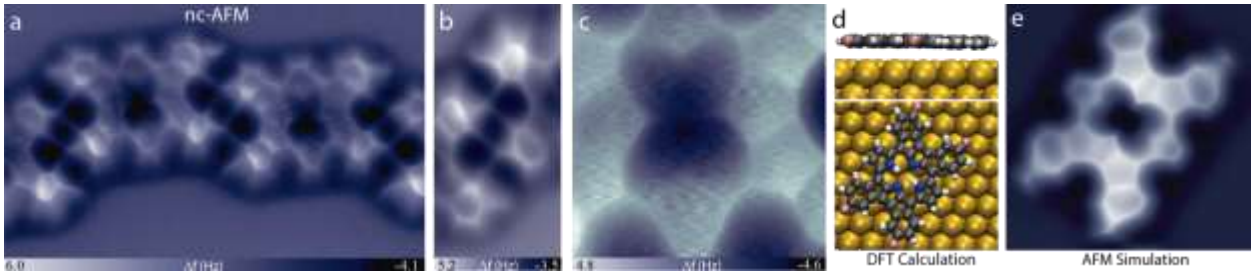

Figure 3. Nature of the 2H-4FPP species on Au(111), revealing the integrity of the C-F bonds and survival of pyrrolic protons. a) nc-AFM image of a one-dimensional supramolecular chain of species A showing the retention of the fluorine atoms at the terminal positions of the peripheral aryl rings. b) High-resolution nc-aFM image showing the different appearances of the C-F and C-H bonds. c) Appearance of the macrocycle of the planarized species A. d) Side and top views of the relaxed model of species A after optimization using DFT. e) Simulated nc-AFM image of a fluorinated A monomer, highlighting the C-F bonds and the appearance of the asymmetric macrocycle. Image size: a) 4.5 x 2.7nm^2, b) 1.1 x 2.2 nm^2, c) 1.0 × 1.0 nm^2.

The first annealing step at 500 K thus planarized the fluorinated porphyrin precursor, but preserved the integrity of the macrocycle and its C-F bonds. No products of intermolecular Ullmann-type coupling reactions were observed, and the process yielded unprecedented supramolecular chains of planarized porphyrin derivatives.

A second annealing step at 575 K induced self-metalation in approximately 20% of the planarized molecules within 30 minutes. Figures 4a-b show zoomed-in images of two planarized macrocycles within a supramolecular chain. The left-hand macrocycle retains its pyrrolic protons but the right-hand one has been self-metalated, resulting in the bright protrusion seen in the constant current and constant height topographs. In addition, although the phenyl substituents are elevated slightly above the rest of the molecular backbone, the macrocycle is clearly visible by nc-AFM (cf. Figure 4c), enabling the observation of its pyrrole moieties. Notably, the metal-organic links between the Au centers and the pyrrole moieties were visualized as unambiguous dark lines. This revealed that the complexed Au centers were tetra-coordinated, as previously shown for planar porphyrin species self-metalated with silver.[19] DFT simulations confirmed the planarity of the metalated species (cf. Figure 4d). The C-F bonds remained intact after this second annealing step and could still be visualized as long rods on the periphery of the porphyrin macrocycles. The on-surface synthesis of Au-4FPP was further supported by the very good agreement between the experimental and simulated nc-AFM images (cf. Figure 4c,e). An unprecedented self-metalation of porphyrins with gold that preserves the ligands' planar conformation was thus achieved by on-surface synthesis. Notably, the Au-4FPP species has an estimated bandgap of ~1.75 eV (cf. Figure 4f), which is slightly greater (by ca. 0.35 eV) than that for the non-metalated species.

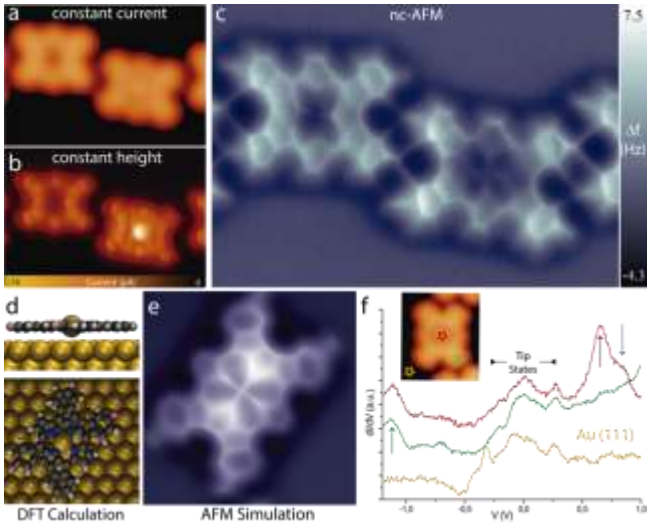

Figure 4. On-surface self-metalation of 2H-4FPP on Au(111) by substrate annealing. a,b) Constant current (a) and constant height (b) STM images of a supramolecular dimer in which the left-hand macrocycle retains its inner protons but the right-hand macrocycle has been self-metalated with a gold center and exhibits a bright protrusion in its inner cavity. c) Simultaneously acquired nc-AFM image of the supramolecular dimer shown in a,b), revealing a bright protrusion in the macrocycle. d) Side and top view of the structure of Au-4FPP on Au(111) obtained by DFT optimization. e) Simulated nc-AFM image of Au-4FPP derivatives, highlighting the cross-like appearance of the macrocycle upon complexation with an Au center. f) STS spectra of Au-4FPP, featuring strong resonances at -1.2eV and 0.65 eV. The spectra plotted in yellow, green, and red were acquired at the positions indicated by the stars of the same color in the inset image. Setting parameters for STS: I_t = 150 pA, V_b = -1.2 V, $V_{modulation}$ = 10 mV, frequency= 773 Hz, integration time = 33 ms per point, sampling energy = 2.5 meV. Image size: a-c) 2.6 × 1.8 nm^2. Scanning parameters: a) V_b = 10 mV, I_t = 15 pA; b) V_b = 10 mV and R_t ~ 1 GΩ.

A third annealing step at 625 K induced the activation of the porphyrins' peripheral C-F and C-H bonds. It is important to note that the competition between C-H and C-F bond activation at fluorocarbons is complex. While the C-H bond is weaker than the C-F bond, the reaction of C-F bonds at the metal surface is usually more exothermic than that of C-H bonds.[43] We did not observe any chemoselectivity: C-F and C-H bonds of adjacent species were activated to similar extents. The cleavage of C-F bonds can be followed by passivation with residual atomic hydrogen, resulting in the formation of defluorinated planarized porphyrin monomers (PPs). Alternatively, it may lead to the formation of planarized porphyrin oligomers via coupling

between adjacent defluorinated C-F or dehydrogenated C-H moieties. Statistically, passivation with hydrogen (~91%) is favored over intermolecular coupling (~9%).

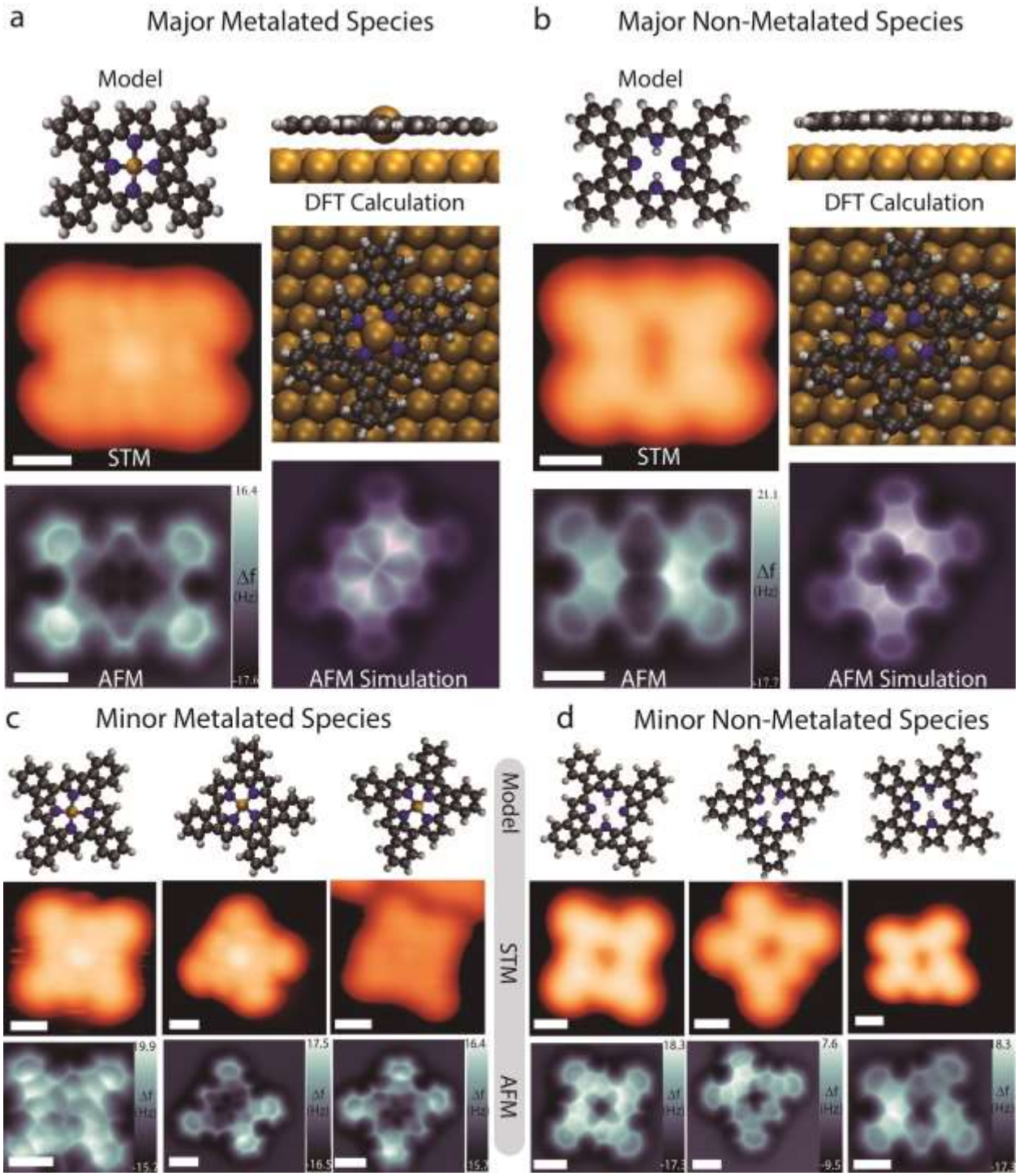

Figure 5. On-surface synthesis of porphyrin planarized monomers (PPs) upon annealing at 625K a submonolayer coverage of 2H-4FTPP on Au(111). a) Model (top left), constant current STM topography image (center left), nc-AFM image (bottom left), DFT simulation of the adsorption conformation (top and middle right), and nc-AFM simulation (bottom right) of a metalated A-type planarized porphyrin (Au-PP). b) Model (top left), constant current STM topography image (center left), nc-AFM image (bottom left), DFT simulation of the adsorption conformation (top and center right), and nc-AFM simulation (bottom right) of a free-base A-type planarized porphyrin species (Au-PP). c) Model (top), STM topography image (middle), and nc-AFM image (bottom) of metalated B-, C-, and D-type planarized porphyrin species (Au-PPs). d) Model (top), STM topography image (middle), and nc-AFM image (bottom) of B-, C-, and D-type free-base planarized porphyrin species (2H-PPs). Scale bars = 5 Å.

Figure 5 shows chemical structures, high resolution scanning probe images, and DFT simulations of selected isolated defluorinated planarized porphyrin monomers (PPs), including both self-metalated (Au-PPs) species and the corresponding free bases (2H-PPs). The structures and conformations of defluorinated species with A-, B-, C-, and D-type structures were revealed by constant height nc-AFM microscopy and comparison to simulations. The imaging results were entirely consistent with the output of the simulations, confirming the loss of fluorine. As discussed above, the C-F bonds of 2H-4FPP are visualized as rod-like structures associated with the pendant aryl moieties in nc-AFM images (cf. Figures 3 and SI5); these rod-like structures are absent in the nc-AFM images of the products obtained after the third annealing step (cf. Figures 5 and SI5). Instead, all of the positions of the phenyl termini are similar in appearance, suggesting that the radicals are passivated with residual hydrogen during annealing or cooling, as is often observed in on-surface syntheses of nanomaterials.[48]

Finally, Figure 6 presents high resolution scanning probe microscopy images revealing the chemical structure of a covalent porphyrin dimer consisting of two metalated A-type planarized porphyrin species. Importantly, the conformations of the porphyrin components in the dimer are identical to those seen in individual monomers. Furthermore, high resolution scanning probe microscopy unambiguously show that the oligomers are formed by single C(F)-C(F) (see Figure 6), C(H)-C(F), or C(H)-C(H) (see Figure SI6) couplings between adjacent phenyl moieties

resulting from the release of terminal fluorine atoms and/or the activation of C-H bonds. The defluorinated carbon centers that do not participate in intermolecular bond formation are passivated by residual atomic hydrogen, as shown in Figure 6 and Figure SI6. The latter figure shows a structure in which one C-F moiety appears to have been retained. The coupling reactions thus exhibit no detectable chemoselectivity. This and the rest of the experimental results suggest that the activation energies of the C-H and C-F bonds of the pendant aryl moieties are quite similar. In addition, the metalation of the macrocycle by a gold adatom had no detectable effect on its coupling reactions because both metalated and free base monomers appeared to undergo coupling with equal facility.

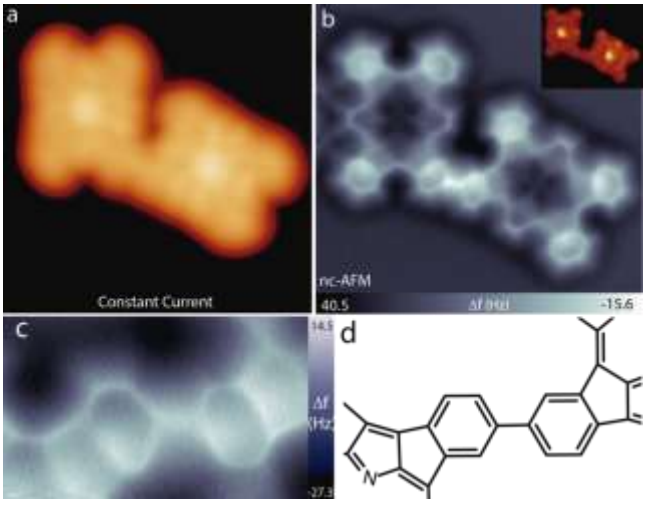

Figure 6. On-surface synthesis of a porphyrin planarized dimer upon annealing at 625K a submonolayer coverage of 2H-4FTPP on Au(111). a,b) High resolution constant current STM topography and nc-AFM image of a dimer of two self-metalated type A planarized porphyrin species. Inset: simultaneously acquired constant height STM image. c) Zoomed-in nc-AFM image confirming the formation of a single C-C bond after annealing. d) Chemical sketch of the resulting bond. Image size: a) 3.4 × 3.4 nm^2; b) 3.0 × 3.4 nm^2; c) 1.2 × 0.7 nm^2. Scanning parameters: a) I_t= 15 pA, V_b = -100 mV, b) Inset: V_b = 10 mV and R_t ~ 1 GΩ.

CONCLUSION

We have demonstrated a strategy for the controlled *in situ* thermal synthesis of complex porphyrin nanoarchitectures from molecular precursors via on-surface processes, which are difficult to be synthesized via standard solution chemistry. This demonstrates the potential of on-surface chemistry to prepare novel chemical compounds with interesting material properties. The intermediates and final products were characterized by high-resolution nc-AFM imaging with a CO-tip, enabling unambiguous determination of their chemical composition. The deposition of 2H-4FTPP on Au(111) resulted in the formation of close-packed islands whose topography and electronic structure were similar to those of non-fluorinated 2H-TPP on Au(111). An initial annealing step at 500 K induced the intramolecular planarization of the deposited precursor to form 4F-TPP on Au(111) via ring-closing reactions between the four pendant phenyl moieties and the macrocycle. This process forms four distinct planar monomers, with the type A monomer predominating. During this process, the activation of C-H bonds at beta and meso positions to afford dehydrogenation and ring closure occurs in preference to C-F defluorination. Remarkably, the use of a fluorinated precursor results in the formation of unprecedented supramolecular chains stabilized by intermolecular CH···FC links. The second annealing step at 575 K affords metalation of the inner macrocycle, and thus the on-surface formation of the long-sought self-metalated gold porphyrins. A final annealing step at 625 K induced defluorination and C-H activation in the pendant aryl moieties, leading to intermolecular coupling reactions that form planarized porphyrin oligomers in which adjacent porphyrin units are linked by C-C single bonds. These oligomers coexist with monomeric planarized porphyrin species. Importantly, the initial planar conformation of the monomers is preserved in the covalently linked oligomers.

These results show that the chemical reactions of surface-confined porphyrins can be controlled by using porphyrin precursors with appropriate molecular designs, and that it is possible to selectively trigger stepwise intra- or inter-molecular reactions by manipulating the annealing temperature. Such on-surface syntheses can enable the creation of unprecedented structures and oligomers, as demonstrated here for gold porphyrin nanoarchitectures. We anticipate that these findings will further the development of the emerging field of on-surface synthesis.

EXPERIMENTAL SECTION

Experiments were performed in a two independent custom designed ultra-high vacuum systems that host a low-temperature Omicron and a Createc scanning tunneling microscope, respectively, where the base pressure was below 5×10^{-10} mbar. All STM images were acquired in constant-current mode with electrochemically etched tungsten tips, applying a bias (V_b) to the sample at a temperature of ~4 K. The Au(111) substrate was prepared by standard cycles of Ar+ sputtering (800 eV) and subsequent annealing at 723 K for 10 minutes. 2H-4FTPP was purchased from Sigma Aldrich and was deposited by organic molecular-beam epitaxy (OMBE) from a quartz crucible maintained at 373 K onto a clean Au(111) at room temperature. The samples were then transferred to the STM stage, which was maintained at 4 K. In AFM imaging, a metal tip mounted on a qplus sensor (resonant frequency ≈ 30 kHz; stiffness ≈ 1800 N/m) was oscillated with a constant amplitude of 50 pm. The tip apex was functionalized with a CO-molecule, and all images were captured in constant height mode.

DFT AND AFM SIMULATIONS

We employed Density Functional Theory calculations using the FHI-AIMS code[49] to different porphyrin derivatives with the Au(111) surface. A model 6x6 supercell, composed of three Au layers was used to represent the Au(111) surface. The single molecule was placed on the surface according to the experimental findings. All the atoms of the slab, except the two bottom Au layers, were allowed to relax until the remaining atomic forces and the total energy were below 10^{-2} eV/Å and 10^{-5} eV respectively. A Monkhorst-Pack grid of 1x1x1 was used for the integration in the Brillouin zone. All the geometry optimizations were performed at the GGA-

PBE[50] level including the Tkatchenko-Scheffler treatment of the van der Waals interactions.[51] The scaled 0th-order regular approximation[52] was applied to consider the relativistic effects.

The AFM images were calculated with Probe Particle code.[53-54] We used the following parameters of the flex- ible probe-particle tip model: the effective lateral stiffness k = 0.24 N/m and effective atomic radius R_C = 1.661 Å. The electrostatic interaction between the molecule and the probe particle was calculated using surface Hartree potential obtained from fully optimized DFT calculations and a quadrupole-like charge distribution at the tip apex to simulate the CO-tip (quadrupole charge of -0.05×0.71^2 e×Å^2).[55]

ASSOCIATED CONTENT

Supporting Information.

The Supporting Information is available free of charge on the ACS Publications website.

Lateral manipulation of 2H-4FPP species on Au(111). Comparison of total energies of different PP products. Partial planarization of 2H-4FTPP on Au(111). Partial planarization and conformation identification of 2H-4FTPP on Au(111). High resolution nc-AFM images of free base and metalated 4FPP and PP species of type A. On-surface formation of porphyrin planarized monomers and oligomers by annealing a submonolayer coverage of 4F-TPP on Au(111) at 625K.

AUTHOR INFORMATION

Corresponding Author

* jelinekp@fzu.cz; david.ecija@imdea.org

Author Contributions

‖ B. Cirera and B. de la Torre contributed equally. All of the authors contributed to the writing of the manuscript and have approved its final version.

ACKNOWLEDGMENT

Work supported by the ERC Consolidator Grant ELECNANO (nº 766555), the EC FP7-PEOPLE-2011-COFUND AMAROUT II program, the Spanish Ramón and Cajal Program (nº RYC-2012-11133), the Spanish Ministerio de Economía y Competitividad (projects FIS 2013-40667-P, FIS 2015-67287-P), the Comunidad de Madrid (projects Y2018/NMT-4783 (QUIMTRONIC-CM), S2013/MIT-3007 (MAD2D), CMS2018/NMT-4321 (NANOMAGCOST)), and the IMDEA Foundation.

P.J. and M.O. acknowledge support from Praemium Academie of the Academy of Science of the Czech Republic, MEYS LM2015087 and GACR 18-09914S and Operational Programme Research, Development and Education financed by European Structural and Investment Funds and the Czech Ministry of Education, Youth and Sports (Projects No. SOLID21 - CZ.02.1.01/0.0/0.0/16_019/0000760 and CZ.02.1.01/0.0/0.0/16_019/0000754).

IMDEA Nanociencia thanks support from the "Severo Ochoa" Programme for Centers of Excellence in R&D (MINECO, Grant SEV-2016-0686).

We acknowledge Willi Auwärter, Francesco Allegretti and Anthoula C. Papageorgiou for fruitful discussions.

REFERENCES

1. Shen, Q.; Gao, H.-Y.; Fuchs, H., Frontiers of on-Surface Synthesis: From Principles to Applications. *Nano Today* 2017, *13*, 77-96.
2. Auwärter, W.; Ecija, D.; Klappenberger, F.; Barth, J. V., Porphyrins at Interfaces. *Nat. Chem.* 2015, *7*, 105-120.
3. Gottfried, J. M., Surface Chemistry of Porphyrins and Phthalocyanines. *Surf. Sci. Rep.* 2015, *70*, 259-379.
4. Jung, T.; Schlittler, R.; Gimzewski, J., Conformational Identification of Individual Adsorbed Molecules with the Stm. *Nature* 1997, *386*, 696-698.

5. Spillmann, H.; Kiebele, A.; Stöhr, M.; Jung, T. A.; Bonifazi, D.; Cheng, F.; Diederich, F., A Two-Dimensional Porphyrin-Based Porous Network Featuring Communicating Cavities for the Templated Complexation of Fullerenes. *Adv. Mater.* 2006, *18*, 275-279.
6. Wintjes, N.; Bonifazi, D.; Cheng, F.; Kibele, A.; Stöhr, M.; Jung, T.; Spillmann, H.; Diederich, F., A Supramolecular Multiposition Rotary Device. *Angew. Chem. Int. Ed.* 2007, *46*, 4089-4092.
7. Shubina, T. E.; Marbach, H.; Flechtner, K.; Kretschmann, A.; Jux, N.; Buchner, F.; Steinrack, H.-P.; Clark, T.; Gottfried, J. M., Principle and Mechanism of Direct Porphyrin Metalation: A Joint Experimental and Theoretical Investigation. *J. Am. Chem. Soc.* 2007, *129*, 9476-9483.
8. Ecija, D.; Trelka, M.; Urban, C.; Mendoza, P. d.; Echavarren, A.; Otero, R.; Gallego, J. M.; Miranda, R., Templated Growth of an Ordered Array of Organic Bidimensional Mesopores. *Appl. Phys. Lett.* 2008, *92*, 223117.
9. Buchner, F.; Seufert, K.; Auwärter, W.; Heim, D.; Barth, J. V.; Flechtner, K.; Gottfried, J. M.; Steinrück, H.-P.; Marbach, H., No-Induced Reorganization of Porphyrin Arrays. *ACS Nano* 2009, *3*, 1789-1794.
10. Écija, D.; Seufert, K.; Heim, D.; Auwärter, W.; Aurisicchio, C.; Fabbro, C.; Bonifazi, D.; Barth, J. V., Hierarchic Self-Assembly of Nanoporous Chiral Networks with Conformationally Flexible Porphyrins. *ACS Nano* 2010, *4*, 4936-4942.
11. Heim, D.; Ecija, D.; Seufert, K.; Auwärter, W.; Aurisicchio, C.; Fabbro, C.; Bonifazi, D.; Barth, J. V., Self-Assembly of Flexible One-Dimensional Coordination Polymers on Metal Surfaces. *J. Am. Chem. Soc.* 2010, *132*, 6783-6790.
12. Écija, D.; Auwärter, W.; Vijayaraghavan, S.; Seufert, K.; Bischoff, F.; Tashiro, K.; Barth, J. V., Assembly and Manipulation of Rotatable Cerium Porphyrinato Sandwich Complexes on a Surface. *Angew. Chem. Int. Ed.* 2011, *50*, 3872-3877.
13. Hanke, F.; Haq, S.; Raval, R.; Persson, M., Heat-to-Connect: Surface Commensurability Directs Organometallic One-Dimensional Self-Assembly. *ACS Nano* 2011, *5*, 9093-9103.
14. Haq, S.; Hanke, F.; Dyer, M. S.; Persson, M.; Iavicoli, P.; Amabilino, D. B.; Raval, R., Clean Coupling of Unfunctionalized Porphyrins at Surfaces to Give Highly Oriented Organometallic Oligomers. *J. Am. Chem. Soc.* 2011, *133*, 12031-12039.
15. Li, Y.; Xiao, J.; Shubina, T. E.; Chen, M.; Shi, Z.; Schmid, M.; Steinrück, H.-P.; Gottfried, J. M.; Lin, N., Coordination and Metalation Bifunctionality of Cu with 5,10,15,20-Tetra(4-Pyridyl)Porphyrin: Toward a Mixed-Valence Two-Dimensional Coordination Network. *J. Am. Chem. Soc.* 2012, *134*, 6401-6408.
16. Bischoff, F.; Seufert, K.; Auwärter, W.; Joshi, S.; Vijayaraghavan, S.; Écija, D.; Diller, K.; Papageorgiou, A. C.; Fischer, S.; Allegretti, F.*, et al.*, How Surface Bonding and Repulsive Interactions Cause Phase Transformations: Ordering of a Prototype Macrocyclic Compound on Ag(111). *ACS Nano* 2013, *7*, 3139-3149.
17. Urgel, J. I.; Ecija, D.; Auwärter, W.; Stassen, D.; Bonifazi, D.; Barth, J. V., Orthogonal Insertion of Lanthanide and Transition-Metal Atoms in Metal–Organic Networks on Surfaces. *Angew. Chem. Int. Ed.* 2015, *54*, 6163-6167.
18. Mielke, J.; Hanke, F.; Peters, M. V.; Hecht, S.; Persson, M.; Grill, L., Adatoms Underneath Single Porphyrin Molecules on Au(111). *J. Am. Chem. Soc.* 2015, *137*, 1844-1849.
19. He, Y.; Garnica, M.; Bischoff, F.; Ducke, J.; Bocquet, M.-L.; Batzill, M.; Auwärter, W.; Barth, J. V., Fusing Tetrapyrroles to Graphene Edges by Surface-Assisted Covalent Coupling. *Nat. Chem.* 2016, *9*, 33.

20. Grill, L.; Dyer, M.; Lafferentz, L.; Persson, M.; Peters, M. V.; Hecht, S., Nano-Architectures by Covalent Assembly of Molecular Building Blocks. *Nat. Nanotechnol.* 2007, *2*, 687-691.
21. Veld, M.; Iavicoli, P.; Haq, S.; Amabilino, D. B.; Raval, R., Unique Intermolecular Reaction of Simple Porphyrins at a Metal Surface Gives Covalent Nanostructures. *Chem. Commun.* 2008, *0*, 1536-1538.
22. Di Santo, G.; Blankenburg, S.; Castellarin-Cudia, C.; Fanetti, M.; Borghetti, P.; Sangaletti, L.; Floreano, L.; Verdini, A.; Magnano, E.; Bondino, F.*, et al.*, Supramolecular Engineering through Temperature-Induced Chemical Modification of 2h-Tetraphenylporphyrin on Ag(111): Flat Phenyl Conformation and Possible Dehydrogenation Reactions. *Chem. Eur. J.* 2011, *17*, 14354-14359.
23. L. Lafferentz; V. Eberhardt; C. Dri; C. Africh; G. Comelli; F. Esch; S. Hecht; Grill, L., Controlling on-Surface Polymerization by Hierarchical and Substrate-Directed Growth. *Nat. Chem.* 2012, *4*, 215-220.
24. van Vörden, D.; Lange, M.; Schmuck, M.; Schaffert, J.; Cottin, M. C.; Bobisch, C. A.; Möller, R., Communication: Substrate Induced Dehydrogenation: Transformation of Octa-Ethyl-Porphyrin into Tetra-Benzo-Porphyrin. *J. Chem. Phys.* 2013, *138*, 211102.
25. Wiengarten, A.; Seufert, K.; Auwärter, W.; Ecija, D.; Diller, K.; Allegretti, F.; Bischoff, F.; Fischer, S.; Duncan, D. A.; Papageorgiou, A. C.*, et al.*, Surface-Assisted Dehydrogenative Homocoupling of Porphine Molecules. *J. Am. Chem. Soc.* 2014, *136*, 9346-9354.
26. Wiengarten, A.; Lloyd, J. A.; Seufert, K.; Reichert, J.; Auwärter, W.; Han, R.; Duncan, D. A.; Allegretti, F.; Fischer, S.; Oh, S. C.*, et al.*, Surface-Assisted Cyclodehydrogenation; Break the Symmetry, Enhance the Selectivity. *Chem. Eur. J.* 2015, *21*, 12285-12290.
27. Saywell, A.; Browning, A. S.; Rahe, P.; Anderson, H. L.; Beton, P. H., Organisation and Ordering of 1d Porphyrin Polymers Synthesised by on-Surface Glaser Coupling. *Chem. Commun.* 2016, *52*, 10342-10345.
28. Ruggieri, C.; Rangan, S.; Bartynski, R. A.; Galoppini, E., Zinc(Ii) Tetraphenylporphyrin on Ag(100) and Ag(111): Multilayer Desorption and Dehydrogenation. *J. Phys. Chem. C* 2016, *120*, 7575-7585.
29. Kim, Y.; Doh, W. H.; Kim, J.; Park, J. Y., In Situ Observations of UV-Induced Restructuring of Self-Assembled Porphyrin Monolayer on Liquid/Au(111) Interface at Molecular Level. *Langmuir* 2018, *34*, 6003-6009.
30. Gross, L.; Schuler, B.; Pavliček, N.; Fatayer, S.; Majzik, Z.; Moll, N.; Peña, D.; Meyer, G., Atomic Force Microscopy for Molecular Structure Elucidation. *Angew. Chem. Int. Ed.* 2018, *57*, 3888-3908.
31. Albrecht, F.; Bischoff, F.; Auwärter, W.; Barth, J. V.; Repp, J., Direct Identification and Determination of Conformational Response in Adsorbed Individual Nonplanar Molecular Species Using Noncontact Atomic Force Microscopy. *Nano Lett.* 2016, *16*, 7703-7709.
32. Marbach, H., Surface-Mediated in Situ Metalation of Porphyrins at the Solid–Vacuum Interface. *Acc. Chem. Res.* 2015, *48*, 2649-2658.
33. Diller, K.; Papageorgiou, A. C.; Klappenberger, F.; Allegretti, F.; Barth, J. V.; Auwarter, W., In Vacuo Interfacial Tetrapyrrole Metallation. *Chem. Soc. Rev.* 2016, *45*, 1629-1656.
34. Chambron, J. C.; Harriman, A.; Heitz, V.; Sauvage, J. P., Ultrafast Photoinduced Electron Transfer between Porphyrinic Subunits within a Bis(Porphyrin)-Stoppered Rotaxane. *J. Am. Chem. Soc.* 1993, *115*, 6109-6114.

35. Knör, G., Intramolecular Charge Transfer Excitation of Meso-Tetrakis (1-Pyrenyl) Porphyrinato Gold(III) Acetate. Photosensitized Oxidation of Guanine. *Inorg. Chem. Commun.* 2001, *4*, 160-163.
36. Zhou, C.-Y.; Chan, P. W. H.; Che, C.-M., Gold(III) Porphyrin-Catalyzed Cycloisomerization of Allenones. *Org. Lett.* 2006, *8*, 325-328.
37. Sun, R. W.-Y.; Che, C.-M., The Anti-Cancer Properties of Gold(III) Compounds with Dianionic Porphyrin and Tetradentate Ligands. *Coord. Chem. Rev.* 2009, *253*, 1682-1691.
38. Che, C.-M.; Sun, R. W.-Y.; Yu, W.-Y.; Ko, C.-B.; Zhu, N.; Sun, H., Gold(III) Porphyrins as a New Class of Anticancer Drugs: Cytotoxicity, DNA Binding and Induction of Apoptosis in Human Cervix Epitheloid Cancer Cells. *Chem. Commun.* 2003, *0*, 1718-1719.
39. Hu, D.; Liu, Y.; Lai, Y.-T.; Tong, K.-C.; Fung, Y.-M.; Lok, C.-N.; Che, C.-M., Anticancer Gold(III) Porphyrins Target Mitochondrial Chaperone HSP60. *Angew. Chem. Int. Ed.* 2016, *55*, 1387-1391.
40. Preiß, S.; Förster, C.; Otto, S.; Bauer, M.; Müller, P.; Hinderberger, D.; Hashemi Haeri, H.; Carella, L.; Heinze, K., Structure and Reactivity of a Mononuclear Gold(II) Complex. *Nat. Chem.* 2017, *9*, 1249.
41. Gross, L.; Mohn, F.; Moll, N.; Liljeroth, P.; Meyer, G., The Chemical Structure of a Molecule Resolved by Atomic Force Microscopy. *Science* 2009, *325*, 1110.
42. Jelínek, P., High Resolution Spm Imaging of Organic Molecules with Functionalized Tips. *J. Phys: Condens. Matter* 2017, *29*, 343002.
43. Eisenstein, O.; Milani, J.; Perutz, R. N., Selectivity of C–H Activation and Competition between C–H and C–F Bond Activation at Fluorocarbons. *Chem. Rev.* 2017, *117*, 8710-8753.
44. Auwärter, W.; Weber-Bargioni, A.; Brink, S.; Riemann, A.; Schiffrin, A.; Ruben, M.; Barth Johannes, V., Controlled Metalation of Self-Assembled Porphyrin Nanoarrays in Two Dimensions. *ChemPhysChem* 2006, *8*, 250-254.
45. Chen, C.; Joshi, T.; Li, H.; Chavez, A. D.; Pedramrazi, Z.; Liu, P.-N.; Li, H.; Dichtel, W. R.; Bredas, J.-L.; Crommie, M. F., Local Electronic Structure of a Single-Layer Porphyrin-Containing Covalent Organic Framework. *ACS Nano* 2018, *12*, 385-391.
46. Parsch, J.; Engels, J. W., C−F···H−C Hydrogen Bonds in Ribonucleic Acids. *J. Am. Chem. Soc.* 2002, *124*, 5664-5672.
47. Di Santo, G.; Blankenburg, S.; Castellarin-Cudia, C.; Fanetti, M.; Borghetti, P.; Sangaletti, L.; Floreano, L.; Verdini, A.; Magnano, E.; Bondino, F.*, et al.*, Supramolecular Engineering through Temperature-Induced Chemical Modification of 2H-Tetraphenylporphyrin on Ag(111): Flat Phenyl Conformation and Possible Dehydrogenation Reactions. *Chem. Eur. J.* 2011, *17*, 14354-14359.
48. Talirz, L.; Ruffieux, P.; Fasel, R., On-Surface Synthesis of Atomically Precise Graphene Nanoribbons. *Adv. Mater.* 2016, *28*, 6222-6231.
49. Blum, V.; Gehrke, R.; Hanke, F.; Havu, P.; Havu, V.; Ren, X.; Reuter, K.; Scheffler, M., Ab Initio Molecular Simulations with Numeric Atom-Centered Orbitals. *Comput. Phys. Commun.* 2009, *180*, 2175-2196.
50. Perdew, J. P.; Burke, W.; Ernzerhof, M., Generalized Gradient Approximation Made Simple. *Phys. Rev. Lett.* 1996, *77*, 3965.
51. Tkatchenko, A.; Scheffler, M., Accurate Molecular Van Der Waals Interactions from Ground-State Electron Density and Free-Atom Reference Data. *Phys. Rev. Lett.* 2009, *102*, 073005.

52. van Lenthe, E.; van Leeuwen, R.; Baerends, E. J.; Snijders, J. G., Relativistic Regular Two-Component Hamiltonians. *Int. J. Quantum. Chem.* 1996, *57*, 281-293.
53. Hapala, P.; Kichin, G.; Wagner, C.; Tautz, F. S.; Temirov, R.; Jelínek, P., Mechanism of High-Resolution Stm/Afm Imaging with Functionalized Tips. *Phys. Rev. B* 2014, *90*, 085421.
54. Hapala, P.; Temirov, R.; Tautz, F. S.; Jelínek, P., Origin of High-Resolution Iets-Stm Images of Organic Molecules with Functionalized Tips. *Phys. Rev. Lett.* 2014, *113*, 226101.
55. Peng, J.; Guo, J.; Hapala, P.; Cao, D.; Ma, R.; Cheng, B.; Xu, L.; Ondráček, M.; Jelínek, P.; Wang, E.*, et al.*, Weakly Perturbative Imaging of Interfacial Water with Submolecular Resolution by Atomic Force Microscopy. *Nat. Commun.* 2018, *9*, 122.